GEOLOGY

Molecular fossils from phytoplankton reveal secular P_{CO_2} trend over the Phanerozoic

Caitlyn R. Witkowski[1]*, Johan W. H. Weijers[2], Brian Blais[3,4], Stefan Schouten[1,5], Jaap S. Sinninghe Damsté[1,5]

Past changes in the atmospheric concentration of carbon dioxide (P_{CO_2}) have had a major impact on earth system dynamics; yet, reconstructing secular trends of past P_{CO_2} remains a prevalent challenge in paleoclimate studies. The current long-term P_{CO_2} reconstructions rely largely on the compilation of many different proxies, often with discrepancies among proxies, particularly for periods older than 100 million years (Ma). Here, we reconstructed Phanerozoic P_{CO_2} from a single proxy: the stable carbon isotopic fractionation associated with photosynthesis (ε_p) that increases as P_{CO_2} increases. This concept has been widely applied to alkenones, but here, we expand this concept both spatially and temporally by applying it to all marine phytoplankton via a diagenetic product of chlorophyll, phytane. We obtained data from 306 marine sediments and oils, which showed that ε_p ranges from 11 to 24‰, agreeing with the observed range of maximum fractionation of Rubisco (i.e., 25 to 28‰). The observed secular P_{CO_2} trend derived from phytane-based ε_p mirrors the available compilations of P_{CO_2} over the past 420 Ma, except for two periods in which our higher estimates agree with the warm climate during those time periods. Our record currently provides the longest secular trend in P_{CO_2} based on a single marine proxy, covering the past 500 Ma of Earth history.

INTRODUCTION

Carbon dioxide shapes climate, breathes life into the biosphere, and turns the cogs of the carbon cycle both in the present and in the past. The past atmospheric concentrations of carbon dioxide (expressed in partial pressure; P_{CO_2}) are reconstructed from indirect measurements (i.e., proxies) such as stomatal densities and indices in plant fossils, the boron isotopic composition of marine carbonate, and the stable carbon isotopic composition ($\delta^{13}C$) of marine phytoplankton, paleosols, and liverworts (1). Each proxy has strengths and limitations, such as its time span of application, associated estimation error, and sensitivity to specific P_{CO_2} levels (2). The reconstruction of secular trends of P_{CO_2} over long time scales [>10 million years (Ma) ago] often relies on compiling many different proxies to generate a continuous record (1). Thus, a single well-constrained proxy that spans the Phanerozoic may strengthen and support our understanding of P_{CO_2}.

The stable carbon isotopic fractionation associated with oxygenic photosynthesis (ε_p) is a proxy that has the potential to span the Phanerozoic. Isotopic fractionation occurs when the CO_2-fixing enzyme Rubisco (ribulose 1,5-biphosphate carboxylase oxygenase) favors ^{12}C over ^{13}C during inorganic carbon fixation, making the photosynthates' isotopic composition ($\delta^{13}C$) depleted in ^{13}C compared to its surrounding environmental CO_2 (3). Higher CO_2 concentrations lead to greater fractionation and vice versa, resulting in a dynamic $\delta^{13}C$ of photoautotrophic biomass (4, 5). This concept is reverse engineered to reconstruct past P_{CO_2} by calculating ε_p from the $\delta^{13}C$ of organic matter (OM) derived from photoautotrophic biomass and the $\delta^{13}C$ of CO_2 derived from fossilized carbonates (e.g., planktonic foraminifera) (6).

ε_p has been extensively tested as a P_{CO_2} proxy since it was first estimated using the $\delta^{13}C$ of geoporphyrins (7) and later using the $\delta^{13}C$ of bulk OM (8). In subsequent studies, factors that influence ε_p other than CO_2 concentrations have been explored in laboratory cultures [e.g., growth rate (9) and cell size (10)] and environmental conditions, such as seasonality, light, and temperature (11). In addition, brought to the forefront in more recent studies, alkenones (and theoretically other phytoplankton) may underestimate P_{CO_2} due to other factors such as cell size and carbon acquisition strategies (12–14). The impact of some factors remains difficult to constrain, such as the assumption that the primary source of carbon is passively diffused $CO_{2[aq]}$ into the cell; under low CO_2 conditions, many phytoplankton implement active uptake of bicarbonate (15), a potential concern given the substantial $\delta^{13}C$ difference between bicarbonate (0‰) and CO_2 (−8‰) (16) and even further complicated by active uptake elevating CO_2 at the site of carboxylation.

The $\delta^{13}C$ of total organic carbon (TOC) to calculate ε_p, in principle, provides a long-term record for P_{CO_2} (8). Using TOC does raise concerns regarding isotopic heterogeneity in different organisms due to kinetic isotope effects and Rayleigh distillation effects with branching points in biosynthetic pathways, leading to distinct $\delta^{13}C$ values for carbohydrates, proteins, and lipids (17). These $\delta^{13}C$ differences among biosynthetic products can be further influenced by diagenetic conditions, such as carbohydrate sulfurization (18), and mixing with terrestrial OM. Abating concerns of using TOC, compound-specific isotope analysis is used on shorter time scales, primarily relying on alkenone biomarkers, the long-chain unsaturated methyl and ethyl n-ketones produced by a select group of Haptophytes. However, ε_p of alkenones only reconstructs P_{CO_2} during the evolutionary history of alkenone-producing Haptophytes, which are not common in the geologic record until the mid-Miocene (19).

To extend the P_{CO_2} reconstruction over the Phanerozoic, we estimated ε_p here using the general phytoplanktonic molecular fossil phytane. Phytane is derived from chlorophyll-a, the omnipresent photoautotrophic pigment that absorbs and transfers light into chemical energy during oxygenic photosynthesis and that has been

[1]Department of Marine Microbiology and Biogeochemistry, NIOZ Royal Netherlands Institute for Sea Research, and Utrecht University, P.O. Box 59, 1790AB Den Burg, Netherlands. [2]Shell Global Solutions International B.V., Grasweg 31, 1031 HW Amsterdam, Netherlands. [3]Department of Science and Technology, College of Arts and Sciences, Bryant University, Smithfield, RI 02917, USA. [4]Institute for Brain and Neural Systems, Brown University, Providence, RI 02912, USA. [5]Department of Earth Sciences, Faculty of Geosciences, Utrecht University, P.O. Box 80.121, 3508 TA Utrecht, Netherlands.
*Corresponding author. Email: caitlyn.witkowski@nioz.nl

present for at least the past 2.15 billion years (Ga) [20]. Phytane has been found in similarly ancient rocks and petroleum [21]. Furthermore, all photosynthetic phytoplankton will contribute to this general biomarker, thereby averaging the ε_p of the phytoplankton community at the time of synthesis. The ε_p calculated from phytane has been previously explored as a proxy for P_{CO_2} at selected sites during specific time periods [22–25] and has been shown to mimic P_{CO_2} trends. Here, we explore its potential for reconstructing secular trends of P_{CO_2} over the Phanerozoic.

RESULTS

We generated $\delta^{13}C$ values of phytane ($\delta^{13}C_{phytane}$) from 41 oils and 29 sediments. Furthermore, we compiled $\delta^{13}C_{phytane}$ values from the literature. New and compiled data yielded 308 data points in total (table S1).

Only marine sediments and oils were used for our compilation to constrain the $\delta^{13}C_{phytane}$ to marine phytoplankton in a more stable and homogenous environment, avoiding the potential decoupling of P_{CO_2} that may occur in local carbon cycles of terrestrial and lacustrine settings. By using only marine settings, this also excludes the additional confounding influence of C_3 and C_4 higher plants; chlorophyll breaks down relatively quickly, eliminating effective transport of terrestrial phytol to the ocean. Immature oils lacking signs of biodegradation were selected on the basis of the confidence in source rock identification to constrain age. Furthermore, these oils were selected on the basis of the lack of terrestrial biomarkers (e.g., oleanane, taraxastane, and bicadinanes) and the lack of local environmental irregularities (e.g., high salinity) to minimize spurious influences on the overall baseline signal for P_{CO_2} (for more details, see Supplementary Text). To attain the general baseline trend for the $\delta^{13}C_{phytane}$ from marine phytoplankton over the Phanerozoic, short-term isotope anomalies were excluded [e.g., carbon isotope excursion events (CIEs) with isotopic spikes of ≥ 2‰ in less than 100 thousand years (ka)] such as the negative CIE of the Paleocene/Eocene boundary [26]. Data before and after CIEs (when the excursion has a clear end point) are included in this compilation.

In our dataset, most $\delta^{13}C_{phytane}$ is from extractable free phytane. Sulfur-bound phytane (i.e., phytane released from sulfur-bound moieties present in sediments that were deposited in anoxic environments) is also included. Sulfur-bound phytane is different than free phytane in that during early diagenesis, inorganic reduced sulfur species selectively react with labile functionalized lipids such as phytol or phytadienes [27]. That is, sulfur-bound phytane is an excellent addition to this record: It may more accurately reflect the $\delta^{13}C$ of the original phytol, whereas free phytane may have small influences by fluctuating inputs of terrestrial OM or archaeal-derived ether lipids [25, 28].

Our compilation shows that over the Phanerozoic, values for the $\delta^{13}C_{phytane}$ range from −34.7 to −23.2‰ (Fig. 1). During the Late Ordovician (455 to 450 Ma), there is a marked negative shift from −28.3 to −34.2‰, followed by a data-scarce Silurian. A gradual positive trend during the Devonian was observed from −33.9‰ at ca. 380 Ma to −28.7‰ at ca. 355 Ma. The Carboniferous into the Early Permian lacks substantial data from which to describe a trend. There is a large decrease from the Permian through the Triassic, from −26.4‰ at ca. 261 Ma to −33.2‰ at ca. 242 Ma. Then, a smaller increase in the Jurassic $\delta^{13}C_{phytane}$, fluctuating between ca. −33 and −30‰, is observed through the Cretaceous. A decrease and a rapid increase are observed in the Late Cretaceous, from −33.0 to −26.8‰ between ca. 98
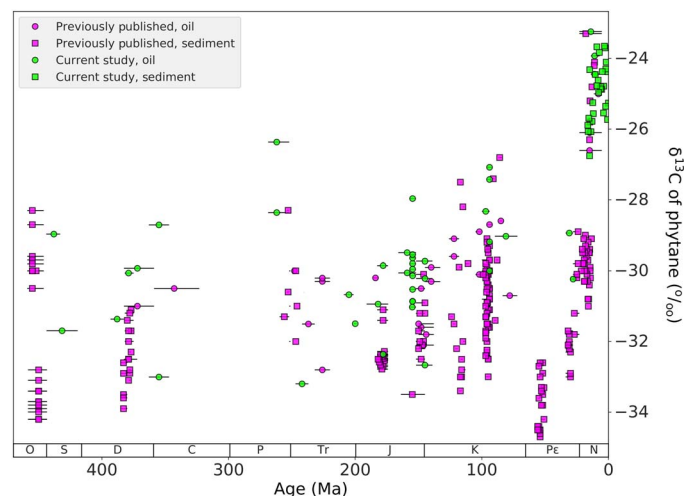

Fig. 1. $\delta^{13}C_{phytane}$. Phanerozoic compilation of the $\delta^{13}C_{phytane}$ from literature (pink) and data from this study (blue), and from sediment (square) and oil (circle). Age uncertainties are shown in the horizontal error bars.

and 93 Ma. The Paleogene shows a similar decrease, followed by an increase from −34.7 to −32.6‰. There is a data gap between 52 and 30 Ma, after which the overall trend continues positive from −33.0 to −25.3‰ at 0.1 Ma, the most positive value in the record of −23.2‰ at 14 Ma.

DISCUSSION

Phytane-derived ε_p

To calculate ε_p, the $\delta^{13}C$ of the photosynthetic biomass (δ_p) and the $\delta^{13}C$ of dissolved CO_2 (δ_d) have to be estimated. δ_p is derived from the $\delta^{13}C_{phytane}$, correcting for the isotopic offset between phytol and biomass. The latter factor was estimated by compiling culture studies from 22 phytoplankton species, yielding an average of 3.3 ± 1.3‰ SD (fig. S1 and Supplementary Text). δ_d is estimated from $\delta^{13}C$ of carbonate, correcting for the carbon isotopic fractionation between dissolved CO_2 with respect to HCO_3^- [16]. Where available (dataset S1), the $\delta^{13}C$ of carbonate is derived from planktonic foraminifera at the same (or nearby) site as the $\delta^{13}C_{phytane}$. Where unavailable, the average $\delta^{13}C$ of carbonate is obtained from the global compiled average of $\delta^{13}C$ of marine planktonic foraminiferal carbonate at the time of deposition [8, 29]. Uncertainty for marine carbonate was assigned ±0.4‰ with uniform distribution. The correction for the isotopic fractionation between dissolved CO_2 with respect to HCO_3^- requires sea surface temperature (SST). This information was obtained from SST proxies (preferably $\delta^{18}O$ from planktonic foraminifera, but otherwise from other proxies such as $U^{k'}_{37}$ or TEX_{86}) measured from each site or nearby site (dataset S1) and assigned a ±4°C SD of uncertainty. Where SST data are unavailable, temperature was estimated by adjusting the modern site for its paleolatitude (using www.paleolatitude. org), finding the SST at that location (e.g., seatemperature.org), and then correcting the present-day SST for global temporal SST anomalies [i.e., 0 to 56 Ma (30, 31) and 65 to 455 Ma (32)]. For further details on the calculations and uncertainty in each parameter on calculated ε_p, see Supplementary Text.

Figure 2 shows that calculated ε_p ranges from ca. 11 to 24‰. The vertical error bars indicate Monte Carlo simulations of uncertainty
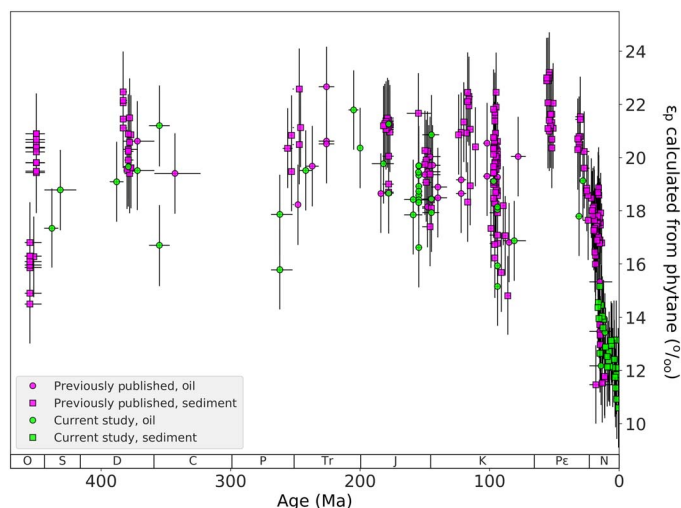
Fig. 2. ε_p calculated from phytane. Phanerozoic ε_p calculated from the $\delta^{13}C_{phytane}$ and $\delta^{13}C$ of dissolved CO_2 estimated from $\delta^{13}C$ of foraminifera from literature (pink) and data from this study (blue), and from sediment (square) and oil (circle). Horizontal error bars indicate dating uncertainty in sample age. Vertical error bars indicate 1 SD (68%) uncertainty in ε_p estimation based on Monte Carlo simulations, culminating the uncertainty in $\delta^{13}C$ of the photosynthetic biomass (based on uncertainty in $\delta^{13}C$ of phytane ± 0.5‰ uniform distribution and the uncertainty in offset between biomass and phytane of 1.3‰ SD) and the $\delta^{13}C$ of dissolved CO_2 (based on uncertainty in $\delta^{13}C$ of planktonic foraminifera ± 0.4‰ uniform distribution and uncertainty in SST ± 4°C SD).

to 1 SD (68%), the culmination of the aforementioned uncertainties within each calculation parameter. The calculated ε_p shows similar trends to the $\delta^{13}C_{phytane}$ in Fig. 1 (side-by-side trends in fig. S2) due to the relatively minor variations in the estimated $\delta^{13}C$ of dissolved CO_2. In this Phanerozoic record, ε_p does not surpass 25‰. This observation matches the theoretical assumption (33) and culture-based observations (9, 34–36) that maximum fractionation (ε_f) for phytoplankton is 25 to 28‰. Because our ε_p is derived from a common phytoplankton biomarker, this 25‰ limit suggests that ε_f is relatively similar among the major taxa. Furthermore, this limit suggests that ε_f has not notably changed over the course of the Phanerozoic, despite the fact that ε_f of Rubisco, when measured in vitro, has found to be substantially lower (e.g., 11‰ in *Emiliania huxleyi*) (37). Young *et al.* (38) show the positive selection of the chloroplast gene that encodes large Rubisco subunits appearing in the evolutionary lineage of ecologically important species (e.g., Chromista, Haptophyta, and Bacillariophyta), likely due to environmental stressors (i.e., during periods of marked PCO_2 declines). Considering that our observed ε_p does not surpass 25‰ over the Phanerozoic, these evolutionary changes to Rubisco may not have made noticeably large changes to ε_f.

Estimates of PCO_2 based on phytane-derived ε_p

To estimate the dissolved carbon dioxide ($CO_{2[aq]}$) from ε_p, we use

$$CO_{2[aq]} = b/(\varepsilon_f - \varepsilon_p) \tag{1}$$

a relationship developed by Hayes (17) and Francois *et al.* (39) and that is a modification of the relationship developed for higher plants from Farquhar *et al.* (40). This concept has been successfully tested in laboratory cultures for $CO_{2[aq]}$ ranging over 0.4 to 79 μmol kg^{-1},

covering CO_2 concentrations lower than the glacial cycles to CO_2 much higher than inferred from the past (10, 36, 41).

The term *b* accounts for all species-specific factors that may influence isotopic fractionation, in particular cell carbon allocation and bicarbonate uptake, as well as cell geometry and growth rate (9), and influencers of growth rate such as nutrient availability (e.g., *b* was found to be empirically related to phosphate concentrations) (42). The factor *b* has almost exclusively been studied in laboratory cultures of Haptophyte algae via alkenones, a relationship then extended into the modern environment (42). In marine surface sediments and suspended matter containing alkenones, *b* ranges from approximately 70 to 240‰ kg μM^{-1} with a mean of 165 ± 53 (42). Given that phytane is a general biomarker averaging the entire phytoplankton community, as opposed to the select group of Haptophytes for alkenones, we calculated *b* from the $\delta^{13}C$ of total OM in diverse modern marine surface sediments (Supplementary Text, table S2, and references therein). Over these 19 study sites, the average for *b* is 168 ± 43‰ kg μM^{-1}, consistent with the alkenone studies and with the *b* value used in previous phytane-based PCO_2 estimations (22, 23). A mean value of 170‰ kg μM^{-1} with an assigned SD of ±60 is used throughout the record. Sensitivity plots (fig. S3A) show that a 1% change in *b* results in a 1% change in PCO_2 estimation. For details on these calculations and uncertainty estimations, please see Supplementary Text.

ε_f is the maximum isotopic fractionation associated with photosynthetic carbon fixation, generally ranging from 25 to 28‰ for algae in modern oceans and laboratory experiments (43, 44). Given that phytane is a general phytoplankton biomarker, the exact percentages of each species in the phytoplankton composition contributing to the phytane pool are needed to estimate the value ε_f, something that cannot be practically achieved for ancient sediments. Thus, we use the average of the laboratory culture ε_f range (26.5 ± 1.5‰ uniform distribution) for the entire phytane-based reconstruction of PCO_2. Sensitivity tests are conducted in Supplementary Text and shown in fig. S3B.

To estimate the atmospheric concentration of carbon dioxide from the $CO_{2[aq]}$, we used

$$PCO_2 = [CO_{2(aq)}]/K_0 \tag{2}$$

based on Henry's law, where the solubility constant K_0, expressed in M/atm, is

$$\ln K_0 = A_1 + A_2(100/T) + A_3\ln(T/100) + S‰[B_1 +$$
$$B_2(T/100) + B_3(T/100)^2] \tag{3}$$

where *A* and *B* are constants, *T* is temperature in Kelvin, and *S*‰ is salinity in ‰ (45). The constants used here are A_{1-3} (−58.0931, 90.5069, and 22.2940) and B_{1-3} (0.02777, −0.02589, and 0.00506), respectively (45). Temperatures are obtained as described above. Salinity is estimated to be 34‰ and assigned a ±2‰ SD uncertainty. Figure 3 shows the consideration of these factors in the error bars of these PCO_2 estimations. The vertical error bars show 1 SD (68%) uncertainty in PCO_2 estimation based on Monte Carlo simulations, culminating the uncertainty in *b* (±60‰ kg μM^{-1} SD), ε_f (±1.5‰), and ε_p (combined uncertainties of $\delta^{13}C$ of phytane ± 0.5‰ uniform distribution, the offset between biomass and phytane of ±1.3‰ SD, $\delta^{13}C$ of planktonic foraminifera ± 0.4‰ uniform distribution, and SST ± 4°C SD). The
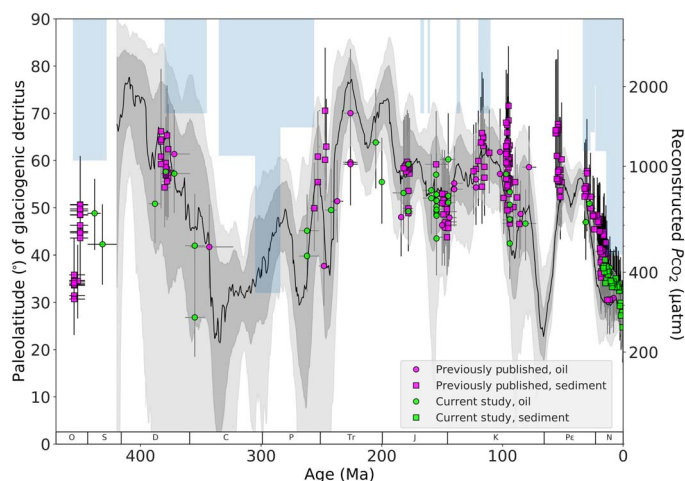
Fig. 3. Phanerozoic P_{CO_2} from phytane. Estimated Phanerozoic P_{CO_2} (on a log scale) from literature (pink) and data from this study (blue), and from sediment (square) and oil (circle). Horizontal error bars indicate uncertainty in age. Vertical error bars indicate 1 SD (68%) uncertainty in P_{CO_2} estimation based on Monte Carlo simulations, culminating the uncertainty in b (±60‰ kg μM^{-1} SD), ε_f (±1.5‰ uniform distribution), and ε_p (combined uncertainty in $\delta^{13}C$ of phytane ± 0.5‰ uniform distribution, the offset between biomass and phytane ± 1.3‰ SD, $\delta^{13}C$ of planktonic foraminifera ± 0.4‰ uniform distribution, and SST ± 4°C SD). Plotted for comparison, the Foster et al. compilation shows the Monte Carlo resampling and LOESS fit of ca. 1500 data points from the five most robust P_{CO_2} proxies: $\delta^{13}C$ of long-chain alkenones, $\delta^{11}B$ of marine carbonate, $\delta^{13}C$ of paleosols, stomatal densities and indices in plants, and $\delta^{13}C$ of liverworts. Sixty-eight percent and 95% confidence intervals are shown in gray and light gray, respectively. The light blue bars represent glacial paleolatitude, as determined by the literature compilation of glaciogenic detritus (46).

impact of uncertainties in these parameters on the final estimated P_{CO_2} is discussed in Supplementary Text and shown in fig. S3C.

The resulting P_{CO_2} values based on $\delta^{13}C_{phytane}$ range from ca. 250 to 1700 μatm (Fig. 3). The estimated P_{CO_2} shows similar trends as $\delta^{13}C_{phytane}$ and ε_p; side-by-side trends in fig. S2 show the similarity of these three different trend lines over the Phanerozoic. For further context, we included the glaciation paleolatitude as determined by glaciogenic detritus compiled by Cather et al. (46) as an indicator of climate (Fig. 3). Last, Fig. 3 includes context for the phytane record by incorporating the compilation of Foster et al. (1), which averages the five most robust P_{CO_2} proxies in current literature: $\delta^{13}C$ of long-chain alkenones, $\delta^{11}B$ of marine carbonate, $\delta^{13}C$ of paleosols, stomatal densities and indices in plants, and $\delta^{13}C$ of liverworts. A comparison between the phytane-based record and the Foster et al. compilation is also shown by time frame (Neogene, Paleogene, Cretaceous, and Phanerozoic) in fig. S4. The phytane-based record here contains ca. 310 estimations, fewer than the ca. 1500 data in the five-proxy Foster et al. compilation, although it does extend more than 50 Ma beyond the current record and has the potential to extend further.

The phytane-based proxy and the Foster et al. compilation show very similar values throughout the entire Phanerozoic. During the Late Ordovician (ca. 460 to 440 Ma), the phytane-based record jumps from ca. 450 to 700 μatm, a more marked shift than seen in the $\delta^{13}C_{phytane}$ and ε_p trends mostly due to the low estimates for temperatures in the Ordovician (ca. 10°C) relative to the estimates for the Devonian (ca. 23°C). The glaciation paleolatitude for this time interval extends to 60° (46), suggesting a cold climate, which agrees with the relatively low P_{CO_2}. From the Devonian into the Early Carboniferous, P_{CO_2} drops

from 1400 to 300 μatm, amplified from the trend seen in phytane-based ε_p but a trend that is similar to the Foster et al. estimations. This significant drop in P_{CO_2} is further supported by the glaciation paleolatitude, where it significantly drops to 60° at the start of the Carboniferous and moves up to 30° by the end of the Carboniferous into the early Permian (46). Then, P_{CO_2} increases from the Late Permian at 450 μatm through the Triassic at 1600 μatm. The Jurassic exhibits a gradual decrease from 1000 μatm during the Toarcian to 600 μatm in the Tithonian. From the Late Jurassic to the mid-Cretaceous, there is a gradual increase to 1300 μatm. The Cenomanian starts at 1500 μatm, the highest P_{CO_2} values for the $\delta^{13}C_{phytane}$-based Phanerozoic record, which then rapidly drops to 600 μatm from ca. 98 to 85 Ma. The high values during the Cenomanian are much higher than those based on the Foster et al. compilation. This may also be attributed to the important role that temperature has when converting raw $\delta^{13}C$ values from biomarkers to P_{CO_2} (see Supplementary Text and fig. S3). However, considering that this period is marked with extremely high SSTs (47), the high phytane-based P_{CO_2} estimations may be appropriate. A second increase and a second drop in the record then occur in the early Paleogene from ca. 56 to 54 Ma, dropping from 1400 to 7500 μatm. Here, our P_{CO_2} estimates are much higher than those of Foster et al. Our high estimates agree with high SST records during this time (48). Last, a decrease in P_{CO_2} from ca. 1000 to 250 μatm is observed from the late Paleogene toward the Holocene (ca. 30 to 0.1 Ma), the lowest estimate for the Phanerozoic. This lowering of CO_2 is supported by the glaciation paleolatitude, which extended as far as 40° (46), and in agreement with the overall cooling observed in bottom water temperatures and the descent in the so-called icehouse world (49).

CONCLUSION

Our Phanerozoic P_{CO_2} record based on the $\delta^{13}C_{phytane}$ is, to the best of our knowledge, one of the longest reconstructions based on a single proxy, extending the known P_{CO_2} record. As a spatially and temporally ubiquitous compound, phytane is one of the most abundantly available phytoplanktonic biomarkers suitable for P_{CO_2} reconstructions, more so considering that both sediments and oils can be used. Among marine-based proxies, this phytane record is the longest reconstruction for P_{CO_2}. Phytane-based P_{CO_2} reconstruction yields similar estimates as compilations of P_{CO_2} proxies, giving the potential to yield a more robust and consistent P_{CO_2} record from a single biomarker.

MATERIALS AND METHODS

The isotopic composition of phytane was measured in 70 marine sediments and oils derived from marine source rocks. Marine oils were processed at Shell Global Solutions International B.V., The Netherlands. Crude oil was eluted over a AgNO$_3$-impregnated silica gel column using three column volumes of cyclohexane to yield saturated hydrocarbon fractions. To remove n-alkanes, the saturated fractions remained in cyclohexane when two layers of 0.5-Å molecular sieve were added to the samples and saturated overnight. The remaining branched/cyclic fractions were injected splitless on gas chromatography–flame ionization detector (GC-FID) at 35°C for 5 min, ramped to 325°C at 4°C/min for 15 min, and held isothermal for another 15 min. A silica capillary column (Ultra-1, 50 m × 0.22 mm; d_f, 0.11 μm) was used with helium as a carrier gas at a constant flow of 25 cm/s. GC–isotope ratio mass spectrometry (IRMS) was conducted using a DB-1ms column (60 m × 0.32 mm; d_f, 0.25 μm). The samples were injected at

220°C into a 70°C oven for 1 min and ramped to 250°C at a rate of 4°C/min and then to 300°C at a rate of 20°C/min for 20 min at a flow rate of 30 cm/s using helium as a carrier gas. The reference gas was normal CO_2 with a predetermined isotopic composition.

Twenty-nine marine sediments from Deep Sea Drilling Project Site 467 offshore of southern California from the Middle Miocene to Lower Pliocene (50) were processed at NIOZ Royal Netherlands Institute for Sea Research, The Netherlands. Powdered sediments (15 to 20 g) were extracted with dichloromethane (DCM):MeOH (9:1, v/v) on a Dionex 250 accelerated solvent extractor at 100°C, 7.6×10^6 Pa. Extracts were eluted over Na_2SO_4 to remove excess water and then over an alumina-packed column to separate polar fractions (DCM:MeOH, 1:1, v/v). Polar fractions were desulfurized using Raney nickel (51), eluted over alumina oxide into an apolar fraction (hexane: DCM, 9:1, v/v), and hydrogenated. Desulfurized apolar fractions were injected on a GC-MS to identify the presence of phytane and on a GC-FID to determine quantity before injection on IRMS for the isotopic composition of phytane. GC-FID, GC-MS, and GC-IRMS all had a starting oven temperature of 70°C and ramped to 130°C at 20°C/min and then to 320°C for 10 min at 4°C/min. GC-IRMS was conducted using a CP-Sil 5 column (25 m × 0.32 mm; d_f 0.12 μm) using a constant flow of He carrier gas.

SUPPLEMENTARY MATERIALS

Supplementary Materials and Methods
Supplementary Text
Fig. S1. Isotopic offset between biomass and phytol.
Fig. S2. Trends from reported $\delta^{13}C_{phytane}$ data to P_{CO_2}.
Fig. S3. Uncertainties associated with equation parameters.
Fig. S4. P_{CO_2} from phytane over the Phanerozoic in time slices.
Table S1. Isotopic offset between biomass and phytol.
Table S2. Estimating b from marine OM in modern-day oceans.
Table S3. Estimating b from phytol across an equatorial Pacific Ocean transect.
Code S1. Python code used for Monte Carlo simulations to calculate uncertainty for P_{CO_2} estimations by considering every parameter involved in the equations.
Data S1. All data used to reconstruct P_{CO_2} from the $\delta^{13}C_{phytane}$.
References (52–96)

REFERENCES AND NOTES

1. G. L. Foster, D. L. Royer, D. J. Lunt, Future climate forcing potentially without precedent in the last 420 million years. *Nat. Commun.* **8**, 14845 (2017).

2. D. L. Royer, Atmospheric CO_2 and O_2 during the Phanerozoic: Tools, patterns, and impacts, in *Treatise on Geochemistry*, H. Holland, K. Turekian, Eds. (Elsevier Science, ed. 2, 2014), vol. 6, pp. 251–267.

3. J. M. Hayes, B. N. Popp, R. Takigiku, M. W. Johnson, An isotopic study of biogeochemical relationships between carbonates and organic-carbon in the greenhorn formation. *Geochim. Cosmochim. Acta* **53**, 2961–2972 (1989).

4. G. D. Farquhar, J. R. Ehleringer, K. T. Hubick, Carbon isotope discrimination and photosynthesis. *Annu. Rev. Plant. Physiol. Plant. Mol. Biol.* **40**, 503–537 (1989).

5. J. M. Hayes, K. H. Freeman, B. N. Popp, C. H. Hoham, Compound-specific isotopic analyses: A novel tool for reconstruction of ancient biogeochemical processes. *Org. Geochem.* **16**, 1115–1128 (1990).

6. K. H. Freeman, J. M. Hayes, Fractionation of carbon isotopes by phytoplankton and estimates of ancient CO_2 levels. *Global Biogeochem. Cycles* **6**, 185–198 (1992).

7. B. N. Popp, R. Takigiku, J. M. Hayes, J. W. Louda, E. W. Baker, The post-Paleozoic chronology and mechanism of ^{13}C depletion in primary marine organic-matter. *Am. J. Sci.* **289**, 436–454 (1989).

8. J. M. Hayes, H. Strauss, A. J. Kaufman, The abundance of ^{13}C in marine organic matter and isotopic fractionation in the global biogeochemical cycle of carbon during the past 800 Ma. *Chem. Geol.* **161**, 103–125 (1999).

9. E. A. Laws, B. N. Popp, R. R. Bidigare, M. C. Kennicutt, S. A. Macko, Dependence of phytoplankton carbon isotopic composition on growth-rate and [Co_2]$_{aq}$: Theoretical

10. B. N. Popp, A. Edward, B. Laws, R. Robert, R. Bidigare, E. John, A. D. Dore, L. Kristi, B. Hanson, C. Stuart, G. Wakeham, Effect of phytoplankton cell geometry on carbon isotopic fractionation. *Geochim. Cosmochim. Acta* **62**, 69–77 (1998).

11. W. M. Sackett, W. R. Eckelmann, M. L. Bender, A. W. H. Bé, Temperature dependence of carbon isotope composition in marine plankton and sediments. *Science* **148**, 235–237 (1965).

12. C. T. Bolton, M. T. Hernández-Sánchez, M.-Á. Fuertes, S. González-Lemos, L. Abrevaya, A. Mendez-Vicente, J.-A. Flores, I. Probert, L. Giosan, J. Johnson, H. M. Stoll, Decrease in coccolithophore calcification and CO_2 since the middle Miocene. *Nat. Commun.* **7**, 10284 (2016).

13. C. T. Bolton, H. M. Stoll, Late Miocene threshold response of marine algae to carbon dioxide limitation. *Nature* **500**, 558–562 (2013).

14. L. M. Mejía, A. Méndez-Vicente, L. Abrevaya, K. T. Lawrence, C. Ladlow, C. Bolton, I. Cacho, H. Stoll, A diatom record of CO_2 decline since the late Miocene. *Earth Planet. Sci. Lett.* **479**, 18–33 (2017).

15. M. R. Badger, T. John Andrews, S. M. Whitney, M. Ludwig, D. C. Yellowlees, W. Leggat, and, G. Dean Price, The diversity and coevolution of Rubisco, plastids, pyrenoids, and chloroplast-based CO_2-concentrating mechanisms in algae. *Can. J. Bot.* **76**, 1052–1071 (1998).

16. W. G. Mook, J. C. Bommerson, W. H. Staverman, Carbon isotope fractionation between dissolved bicarbonate and gaseous carbon-dioxide. *Earth Planet. Sci. Lett.* **22**, 169–176 (1974).

17. J. M. Hayes, Factors controlling ^{13}C contents of sedimentary organic compounds: Principles and evidence. *Mar. Geol.* **113**, 111–125 (1993).

18. J. S. S. Damsté, M. D. Kok, J. Köster, S. Schouten, Sulfurized carbohydrates: An important sedimentary sink for organic carbon? *Earth Planet. Sci. Lett.* **164**, 7–13 (1998).

19. Y. G. Zhang, M. Pagani, Z. H. Liu, S. M. Bohaty, R. DeConto, A 40-million-year history of atmospheric CO_2. *Philos. Trans. A Math. Phys. Eng. Sci.* **371**, 20130096 (2013).

20. B. Rasmussen, I. R. Fletcher, J. J. Brocks, M. R. Kilburn, Reassessing the first appearance of eukaryotes and cyanobacteria. *Nature* **455**, 1101–1104 (2008).

21. C. Li, P. Peng, G. Y. Sheng, J. M. Fu, Y. Z. Yan, A molecular and isotopic geochemical study of Meso- to Neoproterozoic (1.73–0.85 Ga) sediments from the Jixian section, Yanshan Basin, North China. *Precambrian Res.* **125**, 337–356 (2003).

22. K. L. Bice, D. Birgel, P. A. Meyers, K. A. Dahl, K. U. Hinrichs, R. D. Norris, A multiple proxy and model study of Cretaceous upper ocean temperatures and atmospheric CO_2 concentrations. *Paleoceanography* **21**, PA2002 (2006).

23. J. S. S. Damste, M. M. M. Kuypers, R. D. Pancost, S. Schouten, The carbon isotopic response of algae, (cyano)bacteria, archaea and higher plants to the late Cenomanian perturbation of the global carbon cycle: Insights from biomarkers in black shales from the Cape Verde Basin (DSDP Site 367). *Org. Geochem.* **39**, 1703–1718 (2008).

24. B. D. A. Naafs, J. M. Castro, G. A. De Gea, M. L. Quijano, D. N. Schmidt, R. D. Pancost, Gradual and sustained carbon dioxide release during Aptian Oceanic Anoxic Event 1a. *Nat. Geosci.* **9**, 135–139 (2016).

25. E. C. van Bentum, G.-J. Reichart, J. S. S. Damsté, Organic matter provenance, palaeoproductivity and bottom water anoxia during the Cenomanian/Turonian oceanic anoxic event in the Newfoundland Basin (northern proto North Atlantic Ocean). *Org. Geochem.* **50**, 11–18 (2012).

26. P. L. Koch, J. C. Zachos, P. D. Gingerich, Correlation between isotope records in marine and continental carbon reservoirs near the Paleocene/Eocene boundary. *Nature* **358**, 319–322 (1992).

27. W. de Graaf, J. S. S. Damste, J. W. de Deleeuw, Laboratory simulation of natural sulfurization .l. Formation of monomeric and oligomeric isoprenoid polysulfides by low-temperature reactions of inorganic polysulfides with phytol and phytadienes. *Geochim. Cosmochim. Acta* **56**, 4321–4328 (1992).

28. M. P. Koopmans, W. Irene, C. Rijpstra, M. M. Klapwijk, J. W. de Leeuw, M. D. Lewan, J. S. Sinninghe Damsté, A thermal and chemical degradation approach to decipher pristane and phytane precursors in sedimentary organic matter. *Org. Geochem.* **30**, 1089–1104 (1999).

29. A. Barral, B. Gomez, F. Fourel, V. Daviero-Gomez, C. Lécuyer, CO_2 and temperature decoupling at the million-year scale during the Cretaceous Greenhouse. *Sci. Rep.* **7**, 8310 (2017).

30. O. Friedrich, R. D. Norris, J. Erbacher, Evolution of middle to Late Cretaceous oceans— A 55 m.y. record of Earth's temperature and carbon cycle. *Geology* **40**, 107–110 (2012).

31. J. Hansen, M. Sato, G. Russell, P. Kharecha, Climate sensitivity, sea level and atmospheric carbon dioxide. *Philos. Trans. A Math. Phys. Eng. Sci.* **371**, 20120294 (2013).

32. D. L. Royer, R. A. Berner, I. P. Montañez, N. J. Tabor, D. J. Beerling, CO_2 as a primary driver of Phanerozoic climate. *GSA Today* **14**, 4–10 (2004).

33. R. Goericke, J. P. Montoya, B. Fry, Physiology of isotopic fractionation in algae and cyanobacteria, in *Stable Isotopes in Ecology and Environmental Science*, K. Lajtha, R. H. Michener, Eds. (Blackwell, 1994), pp. 187–221.

34. M. Hoins, T. Eberlein, D. B. Van de Waal, A. Sluijs, G. J. Reichart, B. Rost, CO_2-dependent carbon isotope fractionation in dinoflagellates relates to their inorganic carbon fluxes. *J. Exp. Mar. Biol. Ecol.* **481**, 9–14 (2016).

35. B. N. Popp, F. Kenig, S. G. Wakeham, E. A. Laws, R. R. Bidigare, Does growth rate affect ketone unsaturation and intracellular carbon isotopic variability in *Emiliania huxleyi*? *Paleoceanography* **13**, 35–41 (1998).

36. E. B. Wilkes, S. J. Carter, A. Pearson, CO_2-dependent carbon isotope fractionation in the dinoflagellate *Alexandrium tamarense*. *Geochim. Cosmochim. Acta* **212**, 48–61 (2017).

37. A. J. Boller, P. J. Thomas, C. M. Cavanaugh, K. M. Scott, Low stable carbon isotope fractionation by coccolithophore RubisCO. *Geochim. Cosmochim. Acta* **75**, 7200–7207 (2011).

38. J. N. Young, R. E. M. Rickaby, M. V. Kapralov, D. A. Filatov, Adaptive signals in algal Rubisco reveal a history of ancient atmospheric carbon dioxide. *Philos. Trans. R. Soc. Lond. B Biol. Sci.* **367**, 483–492 (2012).

39. R. Francois, M. A. Altabet, R. Goericke, D. C. McCorkle, C. Brunet, A. Poisson, Changes in the $\delta^{13}C$ of surface water particulate organic matter across the subtropical convergence in the SW Indian Ocean. *Global Biogeochem. Cycles* **7**, 627–644 (1993).

40. G. D. Farquhar, M. H. O'Leary, J. A. Berry, On the relationship between carbon isotope discrimination and the inter-cellular carbon-dioxide concentration in leaves. *Aust. J. Plant Physiol.* **9**, 121–137 (1982).

41. E. A. Laws, B. N. Popp, R. R. Bidigare, U. Riebesell, S. Burkhardt, Controls on the molecular distribution and carbon isotopic composition of alkenones in certain haptophyte algae. *Geochem. Geophys. Geosyst.* **2**, 2000GC000057 (2001).

42. R. R. Bidigare, A. Fluegge, K. Freeman, K. Hanson, J. Hayes, D. Hollander, J. Jasper, L. King, E. Laws, J. Milder, F. Millero, R. Pancost, B. Popp, P. Steinberg, S. Wakeham, Consistent fractionation of ^{13}C in nature and in the laboratory: Growth-rate effects in some haptophyte algae. *Global Biogeochem. Cycles* **11**, 279–292 (1997).

43. M. Pagani, M. A. Arthur, K. H. Freeman, Miocene evolution of atmospheric carbon dioxide. *Paleoceanography* **14**, 273–292 (1999).

44. O. Seki, G. L. Foster, D. N. Schmidt, A. Mackensen, K. Kawamura, R. D. Pancost, Alkenone and boron-based Pliocene pCO_2 records. *Earth Planet. Sci. Lett.* **292**, 201–211 (2010).

45. H. R. Weiss, J. A. Cohen, Effects of low-levels of carbon-monoxide on rat-brain and muscle-tissue P02. *Environ. Physiol. Biochem.* **4**, 31–39 (1974).

46. S. M. Cather, N. W. Dunbar, F. W. McDowell, W. C. McIntosh, P. A. Scholle, Climate forcing by iron fertilization from repeated ignimbrite eruptions: The icehouse-silicic large igneous province (SLIP) hypothesis. *Geosphere* **5**, 315–324 (2009).

47. C. L. O'Brien, S. A. Robinson, R. D. Pancost, J. S. Sinninghe Damsté, S. Schouten, D. J. Lunt, H. Alsenz, A. Bornemann, C. Bottini, S. C. Brassell, A. Farnsworth, A. Forster, B. T. Huber, G. N. Inglis, H. C. Jenkyns, C. Linnert, K. Littler, P. Markwic, N. E. Wrobel, Cretaceous sea-surface temperature evolution: Constraints from TEX_86 and planktonic foraminiferal oxygen isotopes. *Earth Sci. Rev.* **172**, 224–247 (2017).

48. J. Frieling, H. Gebhardt, M. Huber, O. A. Adekeye, S. O. Akande, G.-J. Reichart, J. J. Middelburg, S. Schouten, A. Sluijs, Extreme warmth and heat-stressed plankton in the tropics during the Paleocene-Eocene Thermal Maximum. *Sci. Adv.* **3**, e1600891 (2017).

49. J. C. Zachos, G. R. Dickens, R. E. Zeebe, An early Cenozoic perspective on greenhouse warming and carbon-cycle dynamics. *Nature* **451**, 279–283 (2008).

50. L. W. Elrod, B. J. Katz, Organic geochemistry of DSDP Site-467, Middle Miocene to Lower Pliocene strata. *Abstr. Pap. Am. Chem. Soc.* **183**, 57 (1982).

51. J. S. S. Damste, T. I. Eglinton, W. I. C. Rijpstra, J. W. de Leeuw, Characterisation of organically-bound sulfur in high-molecular-weight sedimentary organic matter using flash pyrolysis and Raney Ni desulfurisation, in *Geochemistry of Sulfur in Fossil Fuels*, W. L. Orr, C. M. White, Eds. (American Chemical Society, 1990), pp. 486–528.

52. G. H. Rau, M. A. Arthur, W. E. Dean, N-15/N-14 variations in Cretaceous Atlantic sedimentary sequences: Implication for past changes in marine nitrogen biogeochemistry. *Earth Planet. Sci. Lett.* **82**, 269–279 (1987).

53. C. S. Romanek, E. L. Grossman, J. W. Morse, Carbon isotopic fractionation in synthetic aragonite and calcite: Effects of temperature and precipitation rate. *Geochim. Cosmochim. Acta* **56**, 419–430 (1992).

54. K. Keller, F. M. M. Morel, A model of carbon isotopic fractionation and active carbon uptake in phytoplankton. *Mar. Ecol. Prog. Ser.* **182**, 295–298 (1999).

55. M. K. Eek, M. J. Whiticar, J. K. B. Bishop, C. S. Wong, Influence of nutrients on carbon isotope fractionation by natural populations of Prymnesiophyte algae in NE Pacific. *Deep Sea Res. Part 2 Top Stud. Oceanogr.* **46**, 2863–2876 (1999).

56. R. F. Weiss, Carbon dioxide in water and seawater: The solubility of a non-deal gas. *Mar. Chem.* **2**, 203–215 (1974).

57. B. Alizadeh, H. Saadati, M. Rashidi, M. Kobraei, Geochemical investigation of oils from Cretaceous to Eocene sedimentary sequences of the Abadan Plain, Southwest Iran. *Mar. Petrol. Geol.* **73**, 609–619 (2016).

58. A. Bechtel, U. Movsumova, S. A. I. Strobl, R. F. Sachsenhofer, A. Soliman, R. Gratzer, W. Püttmann, Organofacies and paleoenvironment of the Oligocene Maikop series of Angeharan (eastern Azerbaijan). *Org. Geochem.* **56**, 51–67 (2013).

59. G. Caravaca, C. Thomazo, E. Vennin, N. Olivier, T. Cocquerez, G. Escarguel, E. Fara, J. F. Jenks, K. G. Bylund, D. A. Stephen, A. Brayard, Early Triassic fluctuations of the global carbon cycle: New evidence from paired carbon isotopes in the western USA basin. *Global Planet. Change* **154**, 10–22 (2017).

60. C. Colpaert, B. L. Nikitenko, S. N. Khafaeva, Stratigraphy and ecostratigraphic distribution of foraminiferal morphogroups from the Upper Jurassic of the Makar'yev section (Unzha River; Volga River basin). *Russ. Geol. Geophys.* **58**, 70–86 (2017).

61. A. Delabroye, A. Munnecke, M. Vecoli, P. Copper, N. Tribovillard, M. M. Joachimski, A. Desrochers, T. Servais, Phytoplankton dynamics across the Ordovician/Silurian boundary at low palaeolatitudes: Correlations with carbon isotopic and glacial events. *Palaeogeogr. Palaeoclimatol. Palaeoecol.* **312**, 79–97 (2011).

62. A. Ennyu, M. A. Arthur, M. Pagani, Fine-fraction carbonate stable isotopes as indicators of seasonal shallow mixed-layer paleohydrography. *Mar. Micropaleontol.* **46**, 317–342 (2002).

63. A. Forster, M. M. M. Kuypers, S. C. Turgeon, H.-J. Brumsack, M. R. Petrizzo, J. S. S. Damsté, The Cenomanian/Turonian oceanic anoxic event in the South Atlantic: New insights from a geochemical study of DSDP Site 530A. *Palaeogeogr. Palaeoclimatol. Palaeoecol.* **267**, 256–283 (2008).

64. K. L. French, J. Sepulveda, J. Trabucho-Alexandre, D. R. Gröcke, R. E. Summons, Organic geochemistry of the early Toarcian oceanic anoxic event in Hawsker Bottoms, Yorkshire, England. *Earth Planet. Sci. Lett.* **390**, 116–127 (2014).

65. K. Grice, R. Gibbison, J. E. Atkinson, L. Schwark, C. B. Eckardt, J. R. Maxwell, Maleimides (1*H*-pyrrole-2,5-diones) as molecular indicators of anoxygenic photosynthesis in ancient water columns. *Geochim. Cosmochim. Acta* **60**, 3913–3924 (1996).

66. J. M. Guthrie, Molecular and carbon isotopic analysis of individual biological markers: Evidence for sources of organic matter and paleoenvironmental conditions in the Upper Ordovician Maquoketa Group, Illinois Basin, USA. *Org. Geochem.* **25**, 439–460 (1996).

67. M. Hermoso, P. Pellenard, Continental weathering and climatic changes inferred from clay mineralogy and paired carbon isotopes across the early to middle Toarcian in the Paris Basin. *Palaeogeogr. Palaeoclimatol. Palaeoecol.* **399**, 385–393 (2014).

68. M. R. Hönig, C. M. John, C. Manning, Development of an equatorial carbonate platform across the Triassic-Jurassic boundary and links to global palaeoenvironmental changes (Musandam Peninsula, UAE/Oman). *Gondwana Res.* **45**, 100–117 (2017).

69. W. B. Hughes, A. G. Holba, L. I. P. Dzou, The ratios of dibenzothiophene to phenanthrene and pristane to phytane as indicators of depositional environment and lithology of petroleum source rocks. *Geochim. Cosmochim. Acta* **59**, 3581–3598 (1995).

70. M. M. Joachimski, R. D. Pancost, K. H. Freeman, C. Ostertag-Henning, W. Buggisch, Carbon isotope geochemistry of the Frasnian–Famennian transition. *Palaeogeogr. Palaeoclimatol. Palaeoecol.* **181**, 91–109 (2002).

71. K. G. D. Kochhann, A. Holbourn, W. Kuhnt, J. Xu, Eastern equatorial Pacific benthic foraminiferal distribution and deep water temperature changes during the early to middle Miocene. *Mar. Micropaleontol.* **133**, 28–39 (2017).

72. M. P. Koopmans, J. Köster, H. M. E. Van Kaam-Peters, F. Kenig, S. Schouten, W. A. Hartgers, J. W. de Leeuw, J. S. S. Damsté, Diagenetic and catagenetic products of isorenieratene: Molecular indicators for photic zone anoxia. *Geochim. Cosmochim. Acta* **60**, 4467–4496 (1996).

73. C. Korte, H. W. Kozur, Carbon-isotope stratigraphy across the Permian-Triassic boundary: A review. *J. Asian Earth Sci.* **39**, 215–235 (2010).

74. M. M. M. Kuypers, P. Blokker, E. C. Hopmans, H. Kinkel, R. D. Pancost, S. Schouten, J. S. S. Damsté, Archaeal remains dominate marine organic matter from the early Albian oceanic anoxic event 1b. *Palaeogeogr. Palaeoclimatol. Palaeoecol.* **185**, 211–234 (2002).

75. M. M. M. Kuypers, L. J. Lourens, W. I. C. Rijpstra, R. D. Pancost, I. A. Nijenhuis, J. S. S. Damsté, Orbital forcing of organic carbon burial in the proto-North Atlantic during oceanic anoxic event 2. *Earth Planet. Sci. Lett.* **228**, 465–482 (2004).

76. W. A. Murillo, A. Vieth-Hillebrand, B. Horsfield, H. Wilkes, Petroleum source, maturity, alteration and mixing in the southwestern Barents Sea: New insights from geochemical and isotope data. *Mar. Pet. Geol.* **70**, 119–143 (2016).

77. J. Mutterlose, M. Malkoc, S. Schouten, J. S. S. Damste, A. Forster, TEX_86 and stable $\delta^{18}O$ paleothermometry of early Cretaceous sediments: Implications for belemnite ecology and paleotemperature proxy application. *Earth Planet. Sci. Lett.* **298**, 286–298 (2010).

78. B. Nabbefeld, K. Grice, R. J. Twitchett, R. E. Summons, L. Hays, M. E. Böttcher, M. Asif, An integrated biomarker, isotopic and palaeoenvironmental study through the Late Permian event at Lusitaniadalen, Spitsbergen. *Earth Planet. Sci. Lett.* **291**, 84–96 (2010).

79. A. J. Newell, Rifts, rivers and climate recovery: A new model for the Triassic of England. *Proc. Geol. Assoc.* **129**, 352–371 (2017).

80. E. V. Nunn, G. D. Price, Late Jurassic (Kimmeridgian-Tithonian) stable isotopes ($\delta^{18}O$, $\delta^{13}C$) and Mg/Ca ratios: New palaeoclimate data from Helmsdale, northeast Scotland. *Palaeogeogr. Palaeoclimatol. Palaeoecol.* **292**, 325–335 (2010).

81. M. Pagani, K. H. Freeman, M. A. Arthur, Isotope analyses of molecular and total organic carbon from Miocene sediments. *Geochim. Cosmochim. Acta* **64**, 37–49 (2000).

82. R. D. Pancost, K. H. Freeman, A. D. Herrmann, M. E. Patzkowsky, L. Ainsaar, T. Martma, Reconstructing Late Ordovician carbon cycle variations. *Geochim. Cosmochim. Acta* **105**, 433–454 (2013).

83. J. Sandoval, M. Bill, R. Aguado, L. O'Dogherty, P. Rivas, A. Morard, J. Guexe, The Toarcian in the Subbetic basin (southern Spain): Bio-events (ammonite and calcareous nannofossils)

and carbon-isotope stratigraphy. *Palaeogeogr. Palaeoclimatol. Palaeoecol.* **342–343**, 40–63 (2012).

84. P. L. Schoon, A. Sluijs, J. S. S. Damsté, S. Schouten, Stable carbon isotope patterns of marine biomarker lipids in the Arctic Ocean during Eocene Thermal Maximum 2. *Paleoceanography* **26**, PA3215 (2011).

85. S. Schouten, M. Schoell, W. I. C. Rijpstra, J. S. S. Damsté, J. W. deLeeuw, A molecular stable carbon isotope study of organic matter in immature Miocene Monterey sediments, Pismo basin. *Geochim. Cosmochim. Acta* **61**, 2065–2082 (1997).

86. S. Schouten, H. M. E. Van Kaam-Peters, W. I. C. Rijpstra, M. Schoell, J. S. S. Damste, Effects of an oceanic anoxic event on the stable carbon isotopic composition of Early Toarcian carbon. *Am. J. Sci.* **300**, 1–22 (2000).

87. J. S. Sinninghe Damsté, M. E. L. Kohnen, B. Horsfield, Origin of low-molecular-weight alkylthiophenes in pyrolysates of sulphur-rich kerogens as revealed by micro-scale sealed vessel pyrolysis. *Org. Geochem.* **29**, 1891–1903 (1998).

88. F. C. Tan, J. D. Hudson, M. L. Keith, Jurassic (callovian) paleotemperatures from Scotland. *Earth Planet. Sci. Lett.* **9**, 421–426 (1970).

89. B. J. Tipple, M. Pagani, S. Krishnan, S. S. Dirghangi, S. Galeotti, C. Agnini, L. Giusberti, D. Rio, Coupled high-resolution marine and terrestrial records of carbon and hydrologic cycles variations during the Paleocene–Eocene Thermal Maximum (PETM). *Earth Planet. Sci. Lett.* **311**, 82–92 (2011).

90. H. Tsikos, H. C. Jenkyns, B. Walsworth-Bell, M. R. Petrizzo, A. Forster, S. Kolonic, E. Erba, I. Premoli Silva, M. Baas, T. Wagner, J. S. Sinninghe Damsté, Carbon-isotope stratigraphy recorded by the Cenomanian-Turonian Oceanic Anoxic Event: Correlation and implications based on three key localities. *J. Geol. Soc. London* **161**, 711–719 (2004).

91. S. Tulipani, K. Grice, P. F. Greenwood, P. W. Haines, P. E. Sauer, A. Schimmelmann, R. E. Summons, C. B. Foster, M. E. Böttcher, T. Playton, L. Schwark, Changes of palaeoenvironmental conditions recorded in Late Devonian reef systems from the Canning Basin, Western Australia: A biomarker and stable isotope approach. *Gondwana Res.* **28**, 1500–1515 (2015).

92. E. C. van Bentum, G. J. Reichart, A. Forster, J. S. S. Damste, Latitudinal differences in the amplitude of the OAE-2 carbon isotopic excursion: pCO$_2$ and paleo productivity. *Biogeosciences* **9**, 717–731 (2012).

93. H. M. E. Van Kaam-Peters, S. Schouten, J. W. De Leeuw, J. S. S. Damste, A molecular and carbon isotope biogeochemical study of biomarkers and kerogen pyrolysates of the Kimmeridge Clay Facies: Palaeoenvironmental implications. *Org. Geochem.* **27**, 399–422 (1997).

94. H. M. E. Van Kaam-Peters, S. Schouten, J. Köster, J. S. S. Damste, Controls on the molecular and carbon isotopic composition of organic matter deposited in a Kimmeridgian euxinic shelf sea: Evidence for preservation of carbohydrates through sulfurisation. *Geochim. Cosmochim. Acta* **62**, 3259–3283 (1998).

95. M. Yamamoto, H. Naraoka, R. Ishiwatari, S. Ogihara, Carbon isotope signatures of bacterial 28-norhopanoic acids in Miocene–Pliocene diatomaceous and phosphatic sediments. *Chem. Geol.* **218**, 117–133 (2005).

96. R. A. Berner, S. T. Petsch, J. A. Lake, D. J. Beerling, B. N. Popp, R. S. Lane, E. A. Laws, M. B. Westley, N. Cassar, F. I. Woodward, W. P. Quick, Isotope fractionation and atmospheric oxygen: Implications for Phanerozoic O$_2$ evolution. *Science* **287**, 1630–1633 (2000).

Citation: C. R. Witkowski, J. W. H. Weijers, B. Blais, S. Schouten, J. S. Sinninghe Damsté, Molecular fossils from phytoplankton reveal secular Pco$_2$ trend over the Phanerozoic. *Sci. Adv.* **4**, eaat4556 (2018).